Carbon Dioxide in Montmorillonite Clay Hydrates: Thermodynamics, Structure, and Transport from Molecular Simulation

Alexandru Botan, Benjamin Rotenberg, Virginie Marry, Pierre Turq, Benoit Noetinger

Carbon dioxide in montmorillonite clay hydrates: thermodynamics, structure and transport from molecular simulation

Alexandru Boţan,[*,†,‡] Benjamin Rotenberg,[*,†] Virginie Marry,[†] Pierre Turq,[†] and Benoît Noetinger[‡]

Laboratoire PECSA, UMR 7195, 4 pl. Jussieu, Paris F-75005, France, and 1-4 Avenue de Bois-Préau, Rueil-Malmaison 92852, France

E-mail: alexandru.botan@upmc.fr; benjamin.rotenberg@upmc.fr

Phone: +33 (0)144 273191. Fax: +33 (0)144 273228

[*]To whom correspondence should be addressed
[†]UPMC-Paris6 and CNRS
[‡]IFP

Abstract

We report a Monte Carlo and molecular dynamics simulations study of carbon dioxide in hydrated sodium montmorillonite, including thermodynamical, structural and dynamical properties. In order to simulate the behaviour of a clay caprock in contact with a CO_2 reservoir, we consider clays in equilibrium with H_2O-CO_2 mixtures under conditions close to relevant ones for geological storage, namely a temperature T=348 K, and pressures P=25 and 125 bar, and under which two bulk phases coexist: H_2O-rich liquid on the one hand and CO_2-rich gas (P=25 bar) or supercritical fluid (P=125 bar) on the other hand. We first use grand-canonical MC simulations to determine the number of stable states in clay, their composition and the corresponding equilibrium interlayer distances. The vertical, horizontal and radial distribution functions of the confined mixture, subsequently obtained using molecular dynamics, reveal some structural feature induced by the presence of CO_2. Finally, the simulations indicate that carbon dioxide considerably influences the diffusion of mobile species in clays. We discuss these results by comparing them with those obtained for the bulk mixtures, as well as for Na-montmorillonite in equilibrium with a pure water reservoir water at the same temperature and pressure.

Keywords: carbon dioxide storage, clay minerals, swelling, diffusion, Monte Carlo, molecular dynamics.

Introduction

Clay minerals are of great practical importance in soil science, groundwater hydrology, natural gas and petroleum reservoir engineering, storage of carbon dioxide or toxic chemical and radioactive waste. The role of a clay formation in gas or oil reservoirs is to trap the buoyant fluid in a lower porous formation (often water-filled carbonates). In this context, the most important properties are the low hydraulic permeability of the clay caprock and its ability to retain mobile species. Up to now, the main focus in the literature on CO_2 storage has been on the macrosopic two-phase flow in the host formation, assuming that the integrity of the caprock will be preserved so as to prevent the CO_2 plume from leaking toward the surface. The physics of this transport is very rich, as the introduction of CO_2 perturbs the equilibrium between carbonate rocks and dissolved carbonate ions, which may result in the rock dissolution, pore opening, carbonate reprecipitation, etc.[1,2] The interaction between the CO_2 plume and the clay caprock is also a crucial issue. However, studies on the microscopic scale are necessary to understand the complex interplay between pore size, fluid composition in the pores, and transport of mobile species. Indeed, interactions on the molecular level between water, CO_2 and the clay surface determine how the pore size and composition change when the buoyant bulk water/CO_2 mixture reaches the clay cap-rock. A scenario that one wants to avoid is the dehydration of clay particles induced by the presence of CO_2, leading to their shrinkage. The resulting fractures would then increase the permeability of the caprock, thus reducing its ability to retain the fluid in the reservoir.[3]

These properties depend strongly not only on temperature and pressure, mainly controlled by the burial depth, but also on the clay mineral composition, as was recently discussed by González Sánchez *et al.*[4] For example, the microscopic diffusion coefficient of water, as measured by Quasi-Elastic Neutron scattering, is similar to that of bulk water in compacted kaolinite and pyrophillite (uncharged clays), but considerably smaller in charged clays such as smectites and illites. While all clay minerals are layered aluminosilicates, their structure depends on their charge (neutral or negative), as the latter also implies the presence of compensating counterions between layers. The presence and nature of counterions is a key factor in determining how water and other molecules

might penetrate into the interlayer space, a process generally accompanied by an increase in the interlayer distance and thus known as clay swelling.[5–7] Ab-initio simulations have shown that hydration of clay surfaces is a function of the structure of the crystal lattice.[8–10] Numerous classical molecular simulations and neutron scattering experiments have found strong dependence of swelling and hydration of clay minerals on the interlayer cation size and charge.[11–21] Such interlayer nanopores are absent in uncharged, non-swelling clays, and mobiles species such as water are present only in larger pores between clay particles (stacks of clay layers).

Recently, much attention has been paid to the study of the adsorption of different molecules and ions onto hydrated clay surfaces. These investigations are, in general, experimentally difficult and may be supplemented by using molecular simulation. Molecular simulations have been used to study the atomic-scale interactions between ions and clay surfaces, *e.g.* in the case of uranium sorption[22,23] or cation exchange.[24,25] Adsorption is also possible in the case of methane[26–29] and carbon dioxide,[30] for which stable hydrate complexes were observed experimentally in the presence of smectites under pressures as low as 10 bar and at temperatures as high as 300 K. Titiloye and Skipper[31–33] used molecular simulation to investigate the structure and dynamics for given compositions of methane-water mixtures as interlayer species under pressure and temperature corresponding to reservoir conditions. They observed that an increase in pressure (in the reservoir) or in size of the cations causes a larger swelling and an increase in the self-diffusion coefficient for the methane molecules. Yang and Zhang also reported molecular dynamics simulations of the structure and diffusion coefficient of carbon dioxide in dry, uncharged clay-like slit pores.[34] Cole *et al.* investigated the influence of pressure on the properties of dry supercritical CO_2 in muscovite nanopores, using molecular simulations and small-angle neutron scattering.[35]

However, the above-mentioned simulation studies were carried out at fixed number of molecules, pressure and temperature (*NPT* ensemble) and do not provide information on the amount and composition of the interlayer water-gas mixture, which vary with burial depth and pore size.[36,37] Since it is the chemical potential of the adsorbing molecules (water, methane, carbon dioxide) that is fixed by the reservoir, previous studies of the thermodynamics of clay swelling as a function of

relative humidity have been performed using grand-canonical simulations, i.e. in the $\mu_{H_2O}VT$ ensemble.[14,38] The mixture composition in clays differs from that of the bulk mixture under the same conditions because the phase diagram is modified by the clay/fluid interactions. In order to address this issue, Odriozola *et al* performed simulations in the $\mu_{H_2O}\mu_{C_2H_6}PT$ ensemble to study the behaviour of ethane in hydrated montmorillonite interlayers.[39] This ensemble allows a direct measurement of the water and ethane content in the clay in equilibrium with given reservoir conditions. The ethane concentration observed in the simulations was very low and did not affect the swelling. Since the solubility of carbon dioxide in water is higher than that of ethane and even methane,[30,40] one could expect *a priori* a stronger effect of CO_2 on clay swelling.

In this paper we report a molecular simulation study of carbon dioxide in hydrated interlayers of Na-montmorillonite for two reservoir conditions, with the same temperature T=348 K but different pressures, namely P=25 and 125 bars. The equilibrium interlayer distance and composition are first obtained from Monte Carlo simulations in the $\mu_{H_2O}\mu_{CO_2}VT$ ensemble, where the chemical potentials for water and carbon dioxide correspond to bulk phase coexistence in the reservoir. Molecular Dynamics simulations are then used to investigate the interlayer structure and dynamics.

Computational methods

General strategy

In order to simulate the behaviour of a clay caprock in contact with a CO_2 reservoir, we considered a Na-montmorillonite clay in equilibrium with H_2O-CO_2 mixtures under two sets of P/T conditions close to relevant ones for geological storage, and under which two bulk phases coexist: H_2O-rich liquid and CO_2-rich gas at P=25 bar and T=348.15 K on the the one hand, H_2O-rich liquid and CO_2-rich supercritical fluid at P=125 bar and T=348.15 K, on the other hand. To assess the influence of CO_2 on the thermodynamics, structure and dynamics of hydrated clay we also considered Na-montmorillonite clay in equilibrium with pure water at P=125 bar and 348.15 K.

The grand canonical Monte Carlo method (μVT ensemble) provides an ideal computational

tool for investigating the adsorption of molecules in porous materials.[41,42] In the present work, the clay interlayer exchanges both water and carbon dioxide molecules with reservoirs which set their chemical potentials. The latter are fixed by the coexistence between the CO_2 plume and the liquid H_2O which fills the clay pores (liquid-vapour equilibrium). In the case of the clay phase the pressure has only normal component, therefore the external pressure is also considered as pressure applied normal to the clay surface P^{app}. The equilibrium states of the system, characterized by the interlayer distance z and their composition, correspond to the minimum of the swelling free energy (F):[11]

$$\Delta F = -L_x L_y \int_{z^0}^{z} [P(z') - P^{app}] \mathrm{d}z', \tag{1}$$

where L_x and L_y are the dimensions of the simulation box along x and y axes, respectively. $P(z')$ is the pressure as a function of the interlayer distance z'.

GCMC simulations require the knowledge of the chemical potentials μ_{H_2O} and μ_{H_2O} in the reservoirs. Numerous experimental and numerical works provides the data for pressure, temperature and composition of mixtures under reservoir conditions, but no data is available for the chemical potential. However, the chemical potential can be estimated from these data in μVT ensemble by running a series of simulations at fixed μ_{H_2O} and μ_{CO_2} and choosing the ones which give the right density and composition of the mixture for both coexisting bulk phases.

The equilibrium states are subsequently simulated using Molecular Dynamics to investigate the interlayer structure and dynamics.

Model and methods

The model of clay used in the calculations is the sodium-saturated Wyoming-type montmorillonite with unit formula[43] $Na^{+}_{0.75}[Si_8](Al_{3.25}Mg_{0.75})O_{20}(OH)_4$.

The layered structure of the clay is simulated by two clay layers, using periodic boundary conditions, as done previously *e.g.* in Refs. 11,14,43,44. One of the clay layers is situated in the centre of the simulation box, while the other is divided in two half-layers located at the top

and bottom of the box, as shown in Figure 1. Na^+ cations, water and carbon dioxide molecules are distributed in the interlayer spaces. Each clay layer consists of 8×4 clay unit cells, totalling 1280 atoms, and is treated as a rigid body. The water and carbon dioxide molecules are simulated using the SPC[45] and EPM2[46] models, respectively. The combination of these two models was shown to correctly predict the phase behaviour of H_2O-CO_2 mixtures in the range of pressures and temperatures considered in the present work.[47]

Pairwise additive Lennard-Jones and Coulomb potentials are used to model interactions between particles:

$$U(r_{ij}) = U^{LJ} + U^{C} = 4\varepsilon_{ij}\left[\left(\frac{\sigma_{ij}}{r_{ij}}\right)^{12} - \left(\frac{\sigma_{ij}}{r_{ij}}\right)^{6}\right] + \frac{q_i q_j}{4\pi\varepsilon_0 r_{ij}},$$

where r_{ij} is the distance between sites i and j of different molecules, q_i is the partial charge of the site, σ_{ij} and ε_{ij} are LJ parameters deduced from the conventional Lorentz–Berthelot combining rules.[42] These parameters and charges can be found in references.[44–46,48]

Monte Carlo simulation in the grand canonical ensemble ($\mu_{H_2O}\mu_{CO_2}VT$) were performed using configurational bias techniques (CBMC).[14] The main idea is to divide the trial molecule insertion into two insertion steps: first of the central atom (O for water and C for carbon dioxide), then of other atoms (H or O). We generate k_1 trial configurations for the first atom and select one with probability $p_1 = \exp(-\beta\Delta u_1^{LJ})/W_1$, where $\beta = 1/(k_B T)$, Δu_1^{LJ} is the change in the LJ contribution to the energy produced by the first atom insertion, $W_1 = \sum_{j=1}^{k_1}\exp(-\beta\Delta u_1^{LJ})$ is the Rosenbluth factor. Then we generate k_2 trial configurations for the other atoms. An orientation of the molecule is selected with probability p_2 calculated similarly to p_1, but with Δu_2^{LJ} the change in the LJ contribution to the energy for all atoms of the molecule, except the central one. The same procedure applies for the molecule's removal, though in this case we generate only k-1 trial configuration, since the k^{th} one corresponds to the actual position which must be included in the set of trial

configurations. The acceptance probability for the insertion step reads:

$$P_{acc}^{N\to N+1} = \min\left(1, \frac{V}{\Lambda^3(N+1)}\frac{W_1}{k_1}\frac{W_2}{k_2}\exp[\beta(\mu-\Delta U^C)]\right),$$

and for the removal:

$$P_{acc}^{N\to N-1} = \min\left(1, \frac{\Lambda^3 N}{V}\frac{k_1}{W_1}\frac{k_2}{W_2}\exp[\beta(\Delta U^C-\mu)]\right).$$

Here Λ is the de Broglie wavelength, V the volume of the simulation box, N the number of molecules, μ the chemical potential, and ΔU^C the change in electrostatic energy induced by the molecule insertion (removal). This algorithm was applied for H_2O and CO_2 molecules with $k_1^{H_2O} = k_1^{CO_2} = 50$, $k_2^{H_2O} = 25$ and $k_2^{CO_2} = 50$. The acceptance probability for the translation and rotation steps is based on the standard Metropolis criterion.[49]

The simulations to estimate the chemical potentials from the density and composition of the mixture were performed for both coexisting bulk phases separately in a cubic simulation box. The box size was taken to correspond to 400-500 molecules of H_2O and CO_2 for each considered density. An approximate set of chemical potentials was first obtained by trying 50 $(\mu_{H_2O};\mu_{CO_2})$ pairs in the range [-49:-42]×[-40:-34] kJ/mol. More precise values were then determined by dichotomy (see next section for a discussion of sensitivity). In the case of the clay phase the simulation box corresponds to a periodically replicated parallelepiped with angles adjustable on-the-fly, which allows us to shift clay layers in the horizontal directions without destroying the structure. This is necessary since the relative arrangement of the clay surfaces has been shown to depend on the interlayer distance and content.[13,48] The x-y dimensions of the simulation box are 41.44×35.88 Å^2, and values for z were taken in the range 24 to 35 Å, corresponding to interlayer distances from 12 to 17.5 Å. The spherical cutoff radius is equal to the half of the smallest box side. Long-range electrostatic interactions were computed using Ewald summation.[42] The system was equilibrated for $2\cdot10^7$ steps and $2\cdot10^7$–$5\cdot10^7$ additional steps were used for the calculation of the interlayer composition and pressure.

The pressure is calculated from the expression:

$$P = k_B T \frac{< N^{tot} >}{V} - \frac{1}{L_x L_y} \left\langle \left(\frac{\delta U}{\delta z} \right) \right\rangle . \quad (2)$$

Here N^{tot} is the total number of interlayer molecules, δU the change in configurational energy induced by an infinitesimal change δz in the box size in the z direction (normal to clay layers). The pressure was computed every 100 steps with ghost volume changes δz taken randomly within the range -0.01:0.01 Å. In the case of bulk phases one changes the volume along all directions.[42]

Molecular dynamics simulations were carried out in the canonical ensemble using the DLPOLY software package.[50] Initial configurations were taken from Monte Carlo simulations at the equilibrium distances,with the relative horizontal position of the clay surfaces fixed to the most probable one (as determined from the Monte-Carlo simulations). The equations of motion were integrated using a 1 fs time step and the SHAKE algorithm.[51] The temperature was fixed using a Nosé-Hoover thermostat. Configurations were sampled every 0.1 ps, and the production runs were 3.0 ns. Self-diffusion coefficients along the clay surfaces were calculated using the two-dimensional Einstein relation:

$$D_{\parallel} = \lim_{t \to \infty} \frac{\langle \Delta x(t)^2 + \Delta y(t)^2 \rangle}{4t}, \quad (3)$$

where $< \Delta x(t)^2 >$ is the mean-square displacement of the particle in the x direction.

Results and discussion

Thermodynamics

Monte Carlo simulation in the $\mu_{H_2O}\mu_{CO_2}VT$ ensemble requires the knowledge of the chemical potentials μ_{H_2O} and μ_{CO_2}, which are fixed by the temperature T and pressure P in the reservoir. Thus, we first determined the chemical potentials of water and carbon dioxide so as to obtain in grand-canonical $\mu_{H_2O}\mu_{CO_2}VT$ density and composition of both bulk phases close to experimental data[52,53] and molecular simulations in the Gibbs ensemble.[47] Both quantities are most sensitive to

changes in the chemical potential of CO_2. Depending on the bulk phase (H_2O-rich or CO_2-rich), notable changes are observed either in the density or in the mole fraction. In the liquid H_2O phase a change of 0.25 kJ/mol in μ_{CO_2} leads to changes in mole fraction up to 20 % (in its absolute value) and in density of only 1 %. For the CO_2-rich phase such variations of μ_{CO_2} result in significant density changes (up to 30 %) and negligible changes in the mole fraction (1 %). Changing μ_{H_2O} by 0.25 kJ/mol leads to small changes in density or mole fraction (less 3 %). The retained values for the chemical potential are shown in Table 1. The chemical potential for pure water at T=348.15 K is found with the same approach to be -46.95 kJ/mol. These values were then used for three different sets of GCMC simulations in Na-montmorillonite clay at 348.15 K, corresponding to three different reservoir conditions: 1) pure water at 125 bar, which serves as a reference (before injection of CO_2), 2) CO_2-H_2O mixture at P^{app}=25 bar, and 3) CO_2-H_2O mixture at 125 bar. As can be seen in Table 1, the composition of both phases (CO_2-poor and CO_2-rich) in the reservoir, as well as the density of the CO_2-rich phase (gas vs. supercritical fluid) are not the same at 25 and 125 bar.

Figure 2 shows how the pressure normal to the clay layers varies with the interlayer distance. Each data point, indicated with a symbol, is taken from 1 to 5 independent simulations, while the lines are guides to the eye. A quantitative difference is observed in the first pressure minimum. This results in a larger free energy barrier for the transition from monolayer to bilayer state for the mixture, as shown in Figure 3. We calculated the swelling free energy per unit area for each chosen set of chemical potentials using Eq. (1). For each reservoir condition, there are only two free energy minima points: The first one represents a monolayer state (a layer one molecule thick), the second a bilayer (two molecular layers); all other intermediate states are unstable. They are found for the mixture under 25 bar at 12.3 (monolayer) and 15.4 Å(bilayer), for the mixture under 125 bar at 12.3 and 15.5 Å, and for pure water at 125 bar at 12.4 and 15.3 Å. It should be noted that there is no difference (within the error bars) between pure water and the mixture for bilayer states, while the monolayer spacing is slightly larger for pure water. The bilayer state for all curves is favored with a free energy much lower than that of the monolayer.

The CO_2 interlayer mole fraction for mixtures at 25 and 125 bar are presented in Figure 4. The horizontal lines represent the CO_2 mole fraction in the bulk H_2O-rich phase. In contrast to the reservoir (bulk), there is only one stable phase in the interlayer, with a CO_2 mole fraction larger in the clay phase than in the bulk one. We checked that these results do not depend on the initial composition of the simulated system. From a more quantitative point of view, the monolayer for pure water in the reservoir consists of 6.2 water molecules per sodium ion; for the mixture at 25 bar, 5.2 H_2O and 0.6 CO_2; and for the mixture at 125 bar, 4.9 H_2O and 0.8 CO_2. For the bilayer under the same reservoir conditions we find 11.7 H_2O per Na^+, 11.6 H_2O and 0.3 CO_2, and 11.4 H_2O and 0.6 CO_2, respectively. These data show that the total interlayer density increases with pressure. It should be noted that the number of CO_2 molecules is larger for the monolayer. This observation persists despite very long simulation times and the use of temperature annealing, and is not a simulation artefact. A similar feature was found for an ethane-water mixture in clay.[39] Nevertheless the decrease in CO_2 mole fraction from the monolayer to the bilayer mainly originates from the increase in water molecules.

These equilibrium states determined by grand-canonical Monte-Carlo were then simulated using Molecular Dynamics to investigate the interlayer structure and dynamics. For these simulations, the relative horizontal position of the clay surfaces was fixed to the most probable configuration as determined during the MC simulations and will be discussed bellow.

Structure

Figure 5 displays the density profiles for water oxygen (O_{H_2O}) and hydrogen (H_{H_2O}), carbon dioxide oxygen (O_{CO_2}) and carbon (C) and sodium (Na) atoms perpendicular to clay surface. The data for the mixtures at 25 and 125 bar are very similar and we report only the results at 125 bar. The profiles obtained in the mono- and bilayer cases are compared to the clay system with pure water only. As can be seen from the figure, CO_2 molecules hardly influence the distribution of other atoms. The distance between the C peaks and the surface are almost the same in the mono- and bilayer states. This indicates that C have a tendency to remain close to the clay surface, and is

in line with the absence of increase in the number of interlayer CO_2 from the monolayer to the bilayer case. In the monolayer case, CO_2 molecules are preferentially aligned parallel to the clay surface. The situation changes slightly in the bilayer state, where the peaks of O_{CO_2} atoms do not coincide with that of C atoms. It means that CO_2 molecules are neither parallel nor perpendicular to the surface, despite the fact that contrary to the monolayer case there would be enough space to accommodate a perpendicular orientation.

In order to clarify the situation, we plot in Figure 6 the *x*-*y* distributions for O_{CO_2} and C atoms. The oxygen atoms tend to arrange near the center of the clay hexagonal cavities, whereas C atoms have a small tendency to stay close to O_{clay} atoms. In the bilayer state, one oxygen of the CO_2 molecule enters in the hexagonal cavities, as can be inferred from the location in the *x*-*y* plane of the oxygen atoms that are closest to the surface ($|z| \in [2.0{:}4.5]$ Å see Figure 5). The projected C-O_{CO_2} distances (in the *x*-*y* plane) are different for monolayer and bilayer states, which is in agreement with the density profiles: In the former case the distance is larger and corresponds to CO_2 parallel to the surface, while for the bilayer state CO_2 molecule orientations are distributed rather uniformly around the center of the cavity. These observations are in agreement with MD simulations for carbon dioxide in dehydrated uncharged clays.[34] This means that the charge of the clay surface and the associated presence of counterions and water molecules does not seem to play an important role in this case. Furthermore, horizontal movements of the clay layers, performed using MC simulation, show that in the monolayer case CO_2 molecules fully determine the position of each layer with respect to the other, a feature observed with Sr^{2+} counterions.[13] The preferred position is shown in Figure 6, where the two clay layers are represented by blue and red-yellow hexagons, respectively. Such an arrangement can be explained by the fact, that both oxygen atoms of the same CO_2 molecule tend to arrange near the center of the hexagonal cavity at the same time (one per surface) as illustrated on Figure 6. Note that we have not found any preferred positions for bilayer state. This means that CO_2 molecules near one surface do not influence the position of the second one, and is consistent with the entrance of the CO_2 molecule in the hexagonal cavity.

The radial distribution functions (r.d.f.) for the Na-O_{H_2O}, O_{clay}-C and O_{H_2O}-C pairs for both

interlayer spacings at P=125 bar are shown in Figure 7. Changes in the Na-O_{H_2O} r.d.f. due to the presence of CO_2 are very small. The first peak for O_{H_2O}-C is situated at 3.92 Åin both the clay interlayer and in the bulk phase. The nearest-neighbour coordination number was calculated by integrating over the first peak of the correlation function. C atoms are surrounded by approximately the same number of oxygen atoms for both interlayer hydration state (15.9 for mono- and 16.7 for bilayer, respectively). Interestingly, however, the nature of these atoms differ: There are 4.9 O_{H_2O} and 11 O_{clay} around each carbon atom in the monolayer case, and 11 O_{H_2O} and 5.7 O_{clay} in the bilayer case.

Transport

The transport properties of the interlayer fluid can be characterized by the self-diffusion coefficients of the species parallel to the clay surface ($D_{\|}$). The trajectories obtained from molecular dynamics simulation were analyzed and $D_{\|}$ were calculated as the longtime limiting slope of mean square displacements (MSD) versus time (see Eq. (3)). Table 2 reports the values of the diffusion coefficients calculated from the MSD between 0.5 and 1.0 ns. The standard deviation was calculated over four independent simulations. The experimental diffusion coefficients of H_2O given in Table 2 were obtained by collaborators in synthetic hectorite at T=347 K by neutron spin echo.[54] Although hectorite clay is different from montmorillonite, it has the same swelling properties and gives similar diffusion coefficients at ambient temperature.[55] All data, given in the table for comparison, correspond to P=1 bar. Diffusion coefficients generally decrease with an increase in pressure.[56] This means that the ratio of our simulations over the corresponding experimental data for bulk phase, which is already equal to $\sim$1.4, should probably be higher if we compared with experimental data at higher pressures (see Table 3). This discrepancy can be traced back to the inaccuracy of the SPC model for describing the dynamical properties of water.[57] Nevertheless, we can estimate the influence of CO_2 on the diffusion of interlayer species by analyzing the ratio $D_{\|}/D_{bulk}$, where D_{bulk} are the values of D simulated in the bulk solution. This allows to compare with the previous studies of H_2O-clay systems.[58] In the absence of CO_2, we find that $D_{\|}/D_{bulk}$ for

water and counterions are smaller than in Ref. 58, both in the mono- and bilayer cases, as expected for the higher pressure investigated in the present work.

The results given in Table 2 indicate that the presence of carbon dioxide molecules reduces the mobility of interlayer H_2O and Na^+. To reach this conclusion, one must separate the effect of confinement by the clay layers, which can be deduced from the simulations in the absence of CO_2. This confinement results in a decrease of the diffusion coefficient, relative to the bulk, by a factor ~ 2 in the bilayer and ~ 10 in the monolayer cases, respectively. These values are consistent with the experimental data at 347 K (see Table 2). In the presence of CO_2, this reduction is even more dramatic, with a factor of $\sim$3 for the bilayer, and $\sim$25 for the monolayer. Thus, the diffusion of H_2O and Na^+ in the presence of CO_2 for the monolayer is about 2.5 times smaller than in the absence of CO_2 and only 1.5 times for the bilayer. Since the CO_2 content is higher in the former case (see Figure 4), we conclude that the more CO_2 molecules in the interlayer, the smaller the diffusion coefficient of all species. Such a behaviour is of course not unexpected, as crowding by bulky molecules such as CO_2 hinders the diffusion of other species. Finally, it is worth noting that the smallest $D_{\|}/D_{bulk}$ ratios are obtained for the CO_2 molecules themselves. This can be explained by the apparently stronger interactions of these molecules with the surface, reflected in the molecular profiles discussed in section Structure. Such a behaviour is reminiscent of the observed difference between isovalent cations, for which it has been observed that larger ions (e.g. Cs^+ compared to Na^+) tend to remain closer to the surface than smaller ones, and that their diffusion in the interlayer is more reduced compared to the bulk.[59]

Conclusion

We used grand-canonical Monte Carlo and Molecular Dynamics simulations to study the Na-montmorillonite hydrates in equilibrium with carbon dioxide rich reservoirs. From the μVT study, we determined H_2O and CO_2 contents as a function of the interlayer distances. These results show that the hydrated clay system is capable of adsorbing CO_2 molecules. The swelling free energy

curves indicate that for the considered conditions neither swelling nor shrinkage should be observed. For monohydrated systems containing carbon dioxide, CO_2 molecules lie in the center of interlayers, parallel to the clay surface, and they stabilize a particular position of the clay surfaces relative to each other. For the bilayer, which contains more water molecules but no additional carbon dioxide, the linear O=C=O molecules are located close to the clay surface with one O atom above the center of hexagonal cavities and slightly tilted relative to the surface. The presence of interlayer CO_2 inhibits the diffusion of all the mobile species.

In the future, we will investigate how much the results depend on the force field and describe the system, using *e.g.* the CLAYFF force field.[60,61] Another interesting aspect is the effect of the reservoir composition, taking into account the presence of salt and dissolved HCO_3^- and CO_3^{2-} ions. We are also investigating large (interparticle) pores to clarify the crossover between the surface dominated regime in the interlayer, where only the water-rich phase was found to be stable to the bulk regime where two phases coexist.

Acknowledgement

We thank the Institut Français du Pétrole for permission to publish these results. We are grateful to Prof. J.-P. Hansen, Prof. J.-F. Dufrêche and Dr. C. Nieto-Draghi for valuable discussions.

References

(1) Kaszuba, J. P.; Williams, L. L.; Janecky, D.; Hollis, W.; Tsimpanogiannis, I. *Geochem. Geophys. Geosyst.* **2006**, *7*, Q10003.

(2) Nordbotten, J.; Celia, M.; Bachu, S. *Transp. Porous Med.* **2005**, *58*, 339–360.

(3) Gaus, I. *Int. J. Greenhouse Gas Control* **2010**, *4*, 73–89.

(4) González Sánchez, F.; Juranyi, F.; Gimmi, T.; Van Loon, L.; Unruh, T.; Diamond, L. W. *J. Chem. Phys.* **2008**, *129*, 174706.

(5) Hensen, E.; Smit, B. *J. Phys. Chem. B* **2002**, *106*, 12664–12667.

(6) Smith, D.; Wang, Y.; Chaturvedi, A.; Whitley, H. *J. Phys. Chem. B* **2006**, *110*, 20046–20054.

(7) Arab, M.; Bougeard, D.; Smirnov, K. S. *Phys. Chem. Chem. Phys.* **2003**, *5*, 4699–4707.

(8) Boek, E.; Sprik, M. *J. Phys. Chem. B* **2003**, *107*, 3251–3256.

(9) Tunega, D.; Benco, L.; Haberhauer, G.; Gerzabek, M. H.; Lischka, H. *J. Phys. Chem. B* **2002**, *106*, 11515–11525.

(10) Churakov, S. V. *Geochim. Cosmochim. Ac.* **2007**, *71*, 1130 – 1144.

(11) Shroll, R. M.; Smith, D. E. *J. Chem. Phys.* **1999**, *111*, 9025–9033.

(12) Whitley, H. D.; Smith, D. *J. Chem. Phys.* **2004**, *120*, 5387–5395.

(13) Young, D. A.; Smith, D. E. *J. Phys. Chem. B* **2000**, *104*, 9163–9170.

(14) Hensen, E.; Tambach, T.; Bliek, A.; Smit, B. *J. Chem. Phys.* **2001**, *115*, 3322–3329.

(15) Boulet, P.; Coveney, P.; Stackhouse, S. *Chem. Phys. Lett.* **2004**, *389*, 261–267.

(16) Swenson, J.; Bergman, R.; Howells, W. *J. Chem. Phys.* **2000**, *113*, 2873–2879.

(17) Ferrage, E.; Lanson, B.; Malikova, N.; Plancon, A.; Sakharov, B.; Drits, V. *Chem. Mater* **2005**, *17*, 3499–3512.

(18) Malikova, N.; Cadene, A.; Marry, V.; Dubois, E.; Turq, P.; Zanotti, J.-M.; Longeville, S. *Chem. Phys.* **2005**, *317*, 226 – 235.

(19) Bérend, I.; Cases, J.-M.; François, M.; Uriot, J.-P.; Michot, L.; Masion, F.; Thomas, F. *Clays Clay Miner.* **1995**, *43*, 324–336.

(20) Cases, J.-M.; Bérend, I.; François, M.; Uriot, J.-P.; Michot, L.; Thomas, F. *Clays Clay Miner.* **1997**, *45*, 8–22.

(21) Bordallo, H. N.; Aldridge, L. P.; Churchman, G. J.; Gates, W. P.; Telling, M. T. F.; Kiefer, K.; Fouquet, P.; Seydel, T.; Kimber, S. A. J. *J. Phys. Chem. C* **2009**, *112*, 13982–13991.

(22) Greathouse, J. A.; Cygan, R. T. *Phys. Chem. Chem. Phys.* **2005**, *7*, 3580–3586.

(23) Meleshyn, A.; Azeroual, M.; Reeck, T.; G. Houben, B. R.; Bunnenberg, C. *Environ. Sci. Technol.* **2009**, *43*, 4896–4901.

(24) Teppen, B. J.; Miller, D. M. *Soil Sci. Soc. Am. J.* **2006**, *70*, 31–40.

(25) Rotenberg, B.; Morel, J.-P.; Marry, V.; Turq, P.; Morel-Desrosiers, N. *Geochim. Cosmochim. Ac.* **2009**, *73*, 4034–4044.

(26) Cha, S.; Ouar, H.; Wildeman, T.; Sloan, E. *J. Phys. Chem.* **1988**, *92*, 6492–6494.

(27) Guggenheim, S.; van Groos, A. F. K. *Geology* **2003**, *31*, 653–656.

(28) Park, S.-H.; Sposito, G. *J. Phys. Chem. B* **2003**, *107*, 2281– 2290.

(29) Cygan, R. T.; Guggenheim, S.; van Groos, A. F. K. *J. Phys. Chem. B.* **2004**, *108*, 15141–15149.

(30) Buffett, B. A.; Zatsepina, O. Y. *Mar. Geol.* **2000**, *164*, 69 – 77.

(31) Titiloye, J.; Skipper, N. *Chem. Phys. Lett.* **2000**, *329*, 23–28.

(32) Titiloye, J.; Skipper, N. *Mol. Phys.* **2001**, *99*, 899–906.

(33) Titiloye, J.; Skipper, N. *J. Coll. Interface Sc.* **2005**, *282*, 422–427.

(34) Yang, X.; Zhang, C. *Chem. Phys. Lett.* **2005**, *407*, 427–432.

(35) Cole, D. R.; Chialvo, A. A.; Rother, G.; Vlcek, L.; Cummings, P. T. *Phil. Mag.* **2010**, *90*, 2339–2363.

(36) Paschinger, E.; Levesque, D.; Kahl, G.; Weis, J.-J. *Europhys. Lett.* **2001**, *55*, 178–183.

(37) Sliwinska-Bartkowiak, M.; Sikorski, R.; Sowers, S. L.; Gelb, L. D.; Gubbins, K. E. *Fluid Phase Equilibria* **1997**, *136*, 93–109.

(38) Tambach, T.; Hensen, E.; B.Smit, *J. Phys. Chem. B* **2004**, *108*, 7586–7596.

(39) Odriozola, G.; Aguilar, J. F.; Lopez-Lemus, J. *J. Chem. Phys.* **2004**, *121*, 4266–4275.

(40) Kim, Y.; Lim, B.; Lee, J.; Lee, C. *J. Chem. Eng. Data* **2008**, *53*, 1351 – 1354.

(41) Allen, M. P.; Tildesley, D. J. *Computer Simulation of Liquids*; Clarendon press: Oxford, 1987.

(42) Frenkel, D.; Smit, B. *Understanding molecular simulation: from algorithms to applications, 2d edition*; Academic Press: London, 2002.

(43) Skipper, N. T.; Refson, K.; McConnell, J. D. C. *J. Chem. Phys.* **1991**, *94*, 7434–7445.

(44) Tambach, T. J. Ph.D. thesis, University of Amsterdam: Nieuwe Achtergracht 166, 1018 WV Amsterdam, The Netherlands, 2005.

(45) Berendsen, H. J. C.; Postma, J. P. M.; van Gunsteren, W. F.; Hermans, J. Interaction models for water in relation to protein hydration. *Intermolecular Forces*, Dordrecht, the Netherlands, 1981; pp 331–342.

(46) Harris, J. G.; Yung, K. H. *J. Phys. Chem.* **1995**, *99*, 12021–12024.

(47) Vorholz, J.; Harismiadis, V. I.; Rumpf, B.; Panagiotopoulos, A. Z.; Maurer, G. *Fluid Phase Equilibria* **2000**, *170*, 203 – 234.

(48) Marry, V.; Turq, P.; Cartailler, T.; Levesque, D. *J. Chem. Phys.* **2002**, *117*, 3454.

(49) Metropolis, N.; Rosenbluth, A. W.; Rosenbluth, M. N.; Teller, A. H.; Teller, E. *J. Chem. Phys.* **1953**, *21*, 1087–1092.

(50) Smith, W.; Forester, T.; Todorov, I.; Leslie, M. *The DLPOLY 2 user manual*; CCLRC Daresbury Laboratory: Daresbury, Warrington, UK, 2006.

(51) Ryckaert, J.-P.; Ciccotti, G.; Berendsen, H. *J. Comput. Phys* **1977**, *23*, 327–341.

(52) Wiebe, R. *Chem. Rev.* **1941**, *29*, 475 – 481.

(53) Gillespie, P. C.; Wilson, G. M. *Vapor-Liquid and Liquid-Liquid Equilibria: Water-Methane, Water-Carbon Dioxide, Water-Hydrogen Sulfide, Water-nPentane, Water-Methane-nPentane*; Technical Report RR-48, 1982.

(54) Dubois, E.; Marry, V.; Malikova, N. Articles in progress.

(55) Malikova, N.; Cadene, A.; Dubois, E.; Marry, V.; Durand-Vidal, S.; Turq, P.; Breu, J.; Zanotti, J.-M.; Longeville, S. *J. Phys. Chem. C* **2007**, *111*, 17603 – 17611.

(56) Zhou, J.; Wang, W. *Langmuir* **2000**, *16*, 8063–8070.

(57) Guillot, B. *J. Mol. Liq.* **2002**, *101*, 219–260.

(58) Malikova, N.; Marry, V.; Dufreche, J.-F.; Simon, C.; Turq, P.; Giffaut, E. *Mol. Phys.* **2004**, *102*, 1965 – 1977.

(59) Marry, V.; Turq, P. *J. Phys. Chem. B* **2003**, *107*, 1832–1839.

(60) Cygan, R. T.; Liang, J.-J.; Kalinichev, A. G. *J. Phys. Chem. B* **2004**, *108*, 1255–1266.

(61) Bourg, I. C.; Sposito, G. *Environ. Sci. Technol.* **2010**, *44*, 2085–2091.

(62) Easteal, A.; Price, W.; Woolf, L. A. *J. Chem. Soc.* **1989**, *85*, 1091.

(63) Thomas, W.; Adams, M. *Trans. Faraday Soc.* **1965**, *61*, 668–673.

(64) Robinson, R.; Stokes, R. *Electrolyte solutions*; Butterworths: London, 1959.

Table 1: Estimated chemical potentials in $\mu_{H_2O}\mu_{CO_2}VT$ simulation (bulk phase) for coexistence curve of H_2O-CO_2 mixtures, based on NPT+Gibbs ensemble simulation[47] and experimental data.[52,53] The statistical uncertainties in the last digits are given in parentheses.

	T, (K)	P, (bar)	μ_{H_2O}, (kJ/mol)	μ_{CO_2}, (kJ/mol)	$\rho^{H_2O-rich}$, (g/cm^3)	$x_{CO_2}^{H_2O-rich}$ mole fraction	$\rho^{CO_2 rich}$, (g/cm^3)	$x_{CO_2}^{CO_2-rich}$ mole fraction
Experiment[52,53]	348.15	25.33	–	–	–	0.0055	–	0.9894
	348.15	25.33	–	–	–	0.0054	–	0.9818
	348.15	126.66	–	–	–	–	–	0.9915
Simulation[47]	348.15	25	–	–	0.944(8)	0.0034(13)	0.0401(5)	0.9777(70)
NPT+Gibbs simulation	348.15	125	–	–	0.948(10)	0.0140(24)	0.313(18)	0.9940(8)
$\mu_{H_2O}\mu_{CO_2}VT$	348.15	24.23(7)[a]	-46.85	-39.25	0.934(3)	0.004(1)	0.039(1)	0.982(1)
(this work)	348.15	122.35(98)[a]	-46.85	-35.35	0.940(5)	0.014(1)	0.298(3)	0.994(1)

[a] The pressure was calculated in the CO_2-rich phase.

Table 2: Diffusion coefficient data obtained in this work for the clay phase, T=348.15 K and some of those presented by Malikova *et al*[58] and collaborators.[54] The standard deviations in the last digits are given in parentheses.

	H_2O		Na^+		CO_2	
	$D_\parallel/10^{-9}m^2s^{-1}$	$D_\parallel/D_{bulk}$	$D_\parallel/10^{-9}m^2s^{-1}$	$D_\parallel/D_{bulk}$	$D_\parallel/10^{-9}m^2s^{-1}$	$D_\parallel/D_{bulk}$
Monolayer						
CO_2-H_2O-clay, P=25 bar, this work	0.51 (2)		0.19 (2)		0.24 (4)	
CO_2-H_2O-clay, P=125 bar, this work	0.32 (2)	0.04	0.13 (2)	0.03	0.17 (2)	0.02
H_2O-clay, P=125 bar, this work	0.99 (2)	0.12	0.36 (3)	0.08		
H_2O-clay, T=347 K, experiment[a] [54]	0.75	0.13				
H_2O-clay, T=330 K, simulation[a] [58]	0.83(10)	0.18	0.41(5)			
H_2O-clay, T=375 K, simulation[a] [58]	1.6(1)	0.19	0.70(8)			
Bilayer						
CO_2-H_2O-clay, P=25 bar, this work	3.5 (1)		1.3 (1)		1.6 (2)	
CO_2-H_2O-clay, P=125 bar, this work	3.2 (1)	0.39	1.4 (1)	0.30	1.5 (1)	0.19
H_2O-clay, P=125 bar, this work	3.9 (1)	0.48	2.1 (1)	0.46		
H_2O-clay, T=347 K, experiment[a] [54]	2.1	0.35				
H_2O-clay, T=320 K, simulation[a] [58]	2.0	0.56	1.3(1)			
H_2O-clay, T=360 K, simulation[a] [58]	4.2	0.60	3.7(5)			

[a] P=1 bar.

Table 3: Diffusion coefficient data obtained in this work for the bulk phase, T=348.15 K and some of those presented by Easteal *et al*,[62] Thomas and Adams.[63] The standard deviations in the last digits are given in parentheses.

	H_2O $D/10^{-9}m^2s^{-1}$	Na^+ $D/10^{-9}m^2s^{-1}$	CO_2 $D/10^{-9}m^2s^{-1}$
CO_2-H_2O, P=125 bar, this work	8.2 (1)		
Na^+ in water, P=125 bar, this work	8.1 (1)	4.6 (4)	
H_2O, T=343 K, experiment[a] [62]	5.646		
H_2O, T=353 K, experiment[a] [62]	6.582		
Na^+ in water[ab]		3.5	
CO_2-H_2O, experiment[a] [63]			5.4 (1)

[a] P=1 bar; [b] D was estimated from the experimental data for the electrical conductivity.[64]

Figure 1: Schematic representation of the simulation box.

Figure 2: Pressure as a function of the interlayer distance at T = 348.15 K. The black solid, red dashed and blue dashed-dotted lines are interpolations of the data points for reservoir conditions corresponding to the mixture at 25, 125 bar and pure water at 125 bar, respectively.

Figure 3: Clay swelling free energy per unit area plotted as a function of the interlayer distance.

Figure 4: CO_2 mole fraction plotted as a function of interlayer distance for Na^+- montmorillonite at T=348.15 K. The horizontal lines indicate the CO_2 mole fraction in the bulk H_2O-rich phase. The grey stripes visualize the location of the stable states.

Figure 5: Density profiles of the C, O, H and Na atoms for the mixture (first column) and pure water (second column) at P=125 bar, T=348.15 K. The first and second rows correspond the monolayer and bilayer states, respectively. The vertical dashed lines represent the clay surface oxygen atoms.

Figure 6: Distribution of O_{CO_2}(left) and C(right) atoms parallel to the clay surface. Light regimes correspond to high density. The first and second rows correspond the monolayer and bilayer states, respectively. In the monolayer case, a typical configuration of the CO_2 molecule is indicated. In the bilayer case, results for O_{CO_2} correspond only to the atom closest to the surface ($|z| \in$[2.0:4.5] Å see Figure 5). Results are given for one unit cell with dimensions $a \times b$ = 5.18 $\times$ 8.97 Å^2 . Oxygen surface atoms are indicated for one clay surface by red circles, silicon atoms by yellow circles. The location of the second surface is indicated by the blue hexagons.

Figure 7: Radial distribution functions. Results are compared to a bulk ionic solution for Na-H_2O, and to the bulk CO_2-poor liquid for O_{H_2O}-C.

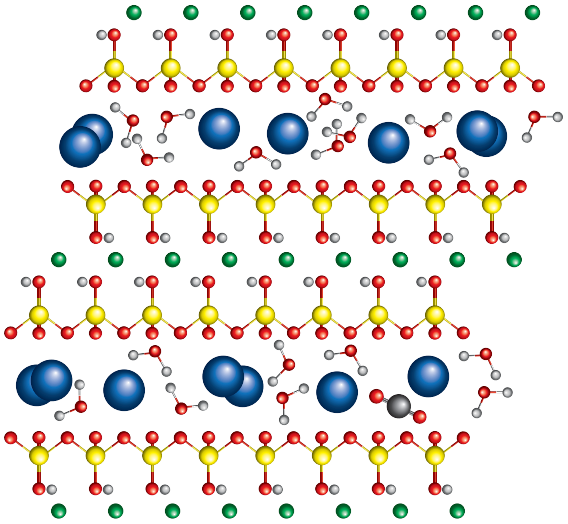

Figure 1.

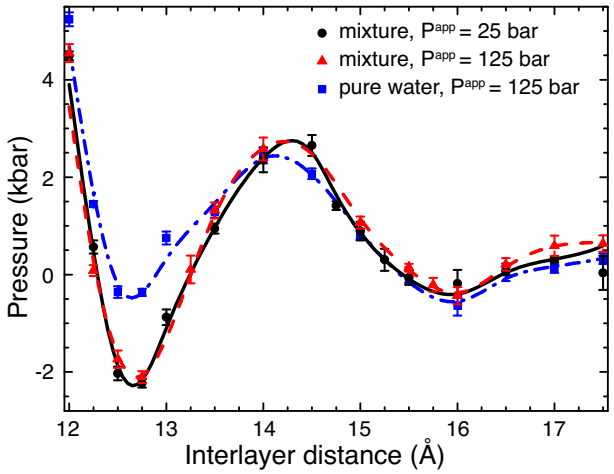
mixture, P^app = 25 bar
mixture, P^app = 125 bar
pure water, P^app = 125 bar
Pressure (kbar)
Interlayer distance (Å)
4
2
0
-2
12
13
14
15
16
17

Figure 2.

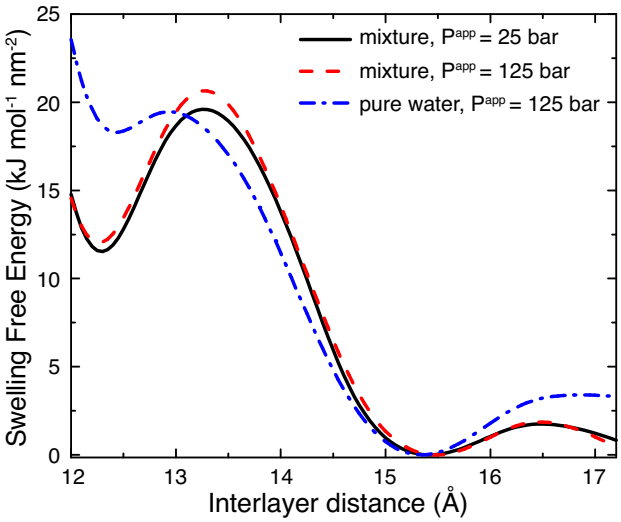
mixture, P^app = 25 bar
mixture, P^app = 125 bar
pure water, P^app = 125 bar
Swelling Free Energy (kJ mol-1 nm-2)
Interlayer distance (Å)
0
5
10
15
20
25
12
13
14
15
16
17

Figure 3.

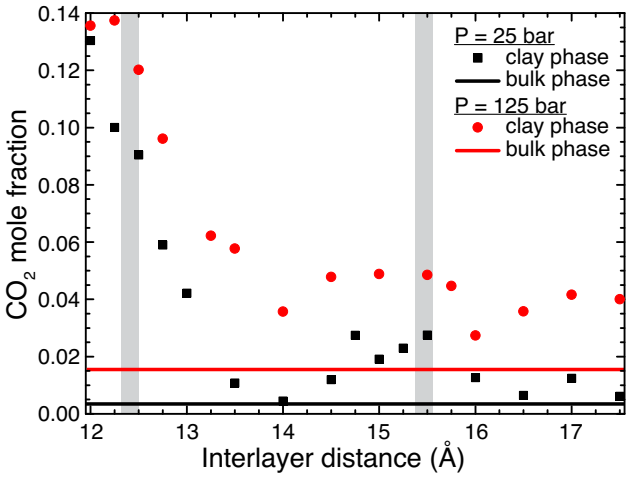
0.14
0.12
0.10
0.08
0.06
0.04
0.02
0.00
CO2 mole fraction
12
13
14
15
16
17
Interlayer distance (Å)
P = 25 bar
clay phase
bulk phase
P = 125 bar
clay phase
bulk phase

Figure 4.

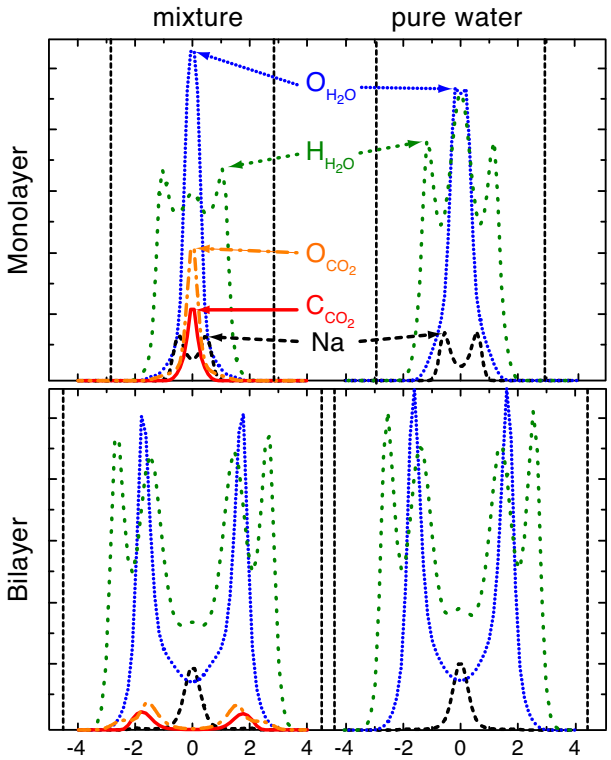
mixture
pure water
Monolayer
Bilayer
O_{H_2O}
H_{H_2O}
O_{CO_2}
C_{CO_2}
Na
-4
-2
0
2
4
-4
-2
0
2
4

Figure 5.

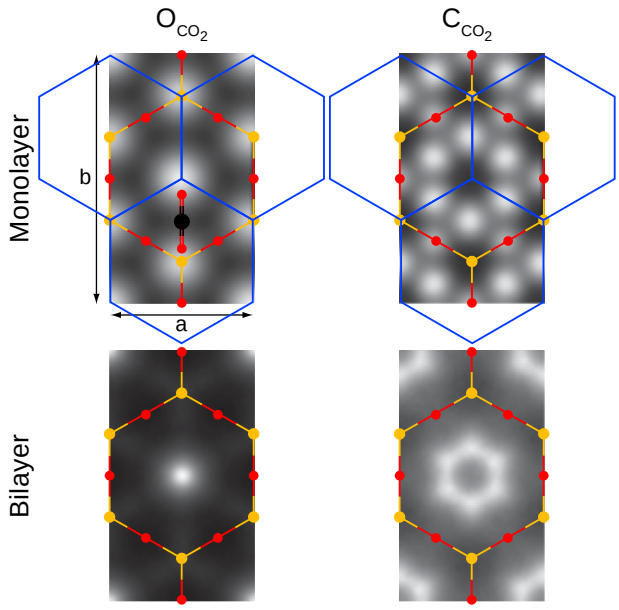

Figure 6.

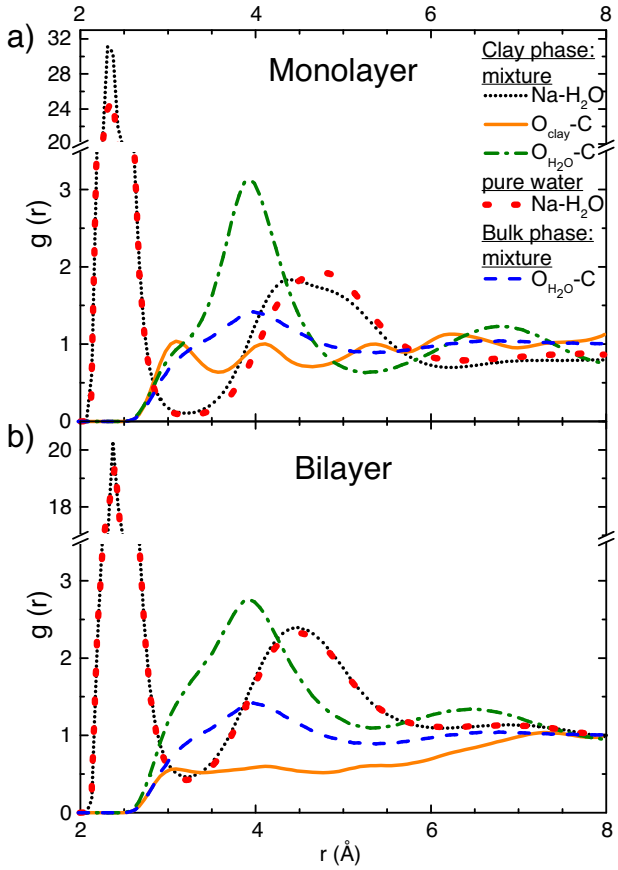
a)
Monolayer
Clay phase:
mixture
Na-H2O
Oclay-C
OH2O-C
pure water
Na-H2O
Bulk phase:
mixture
OH2O-C
g (r)
b)
Bilayer
g (r)
r (Å)

Figure 7.

Graphical TOC Entry